TITLE

NAME Regional Radar Network 2-D Near-Surface Reflectivity and Rain Rate Composites

Version 2.1

Last Updated 25 June 2007

AUTHORS

Timothy J. Lang, PI
Department of Atmospheric Science
Colorado State University
200 W Lake St
Fort Collins, CO 80523
tlang@atmos.colostate.edu
(970) 491-6944

Rit Carbone, PI
NCAR
carbone@ucar.edu

Steven A. Rutledge, Co-PI
CSU Atmospheric Science
rutledge@atmos.colostate.edu

David Ahijevych, Co-I
NCAR/MMM
ahijevyc@ucar.edu
(303) 497-8922

Stephen W. Nesbitt, Co-I
Department of Atmospheric Sciences
University of Illinois at Urbana-Champaign
snesbitt@uiuc.edu

Refer data questions to either Timothy Lang or David Ahijevych

1.0 DATA SET OVERVIEW

This README assumes some basic understanding of meteorological radars, in particular Doppler and polarimetric radars. If you need more complete radar references, the Battan (1973), Doviak and Zrnic (1993), and Bringi and Chandrasekar (2000) textbooks are recommended.

This dataset includes two-dimensional gridded regional composites of near-surface radar reflectivity factor and rain rate from the NAME radar network, which consisted of three radars located near the mouth of the Gulf of California and the western slope of the Sierra Madre Occidental. The locations of these radars are shown in Fig. 1.

The three radars are:

1) S-Pol – 23.9290 N, 106.9521 W, 20 m MSL
2) Cabo – 22.8971 N, 109.9272 W, 281 m MSL
3) Guasave – 25.5676 N, 108.4633 W, 85 m MSL

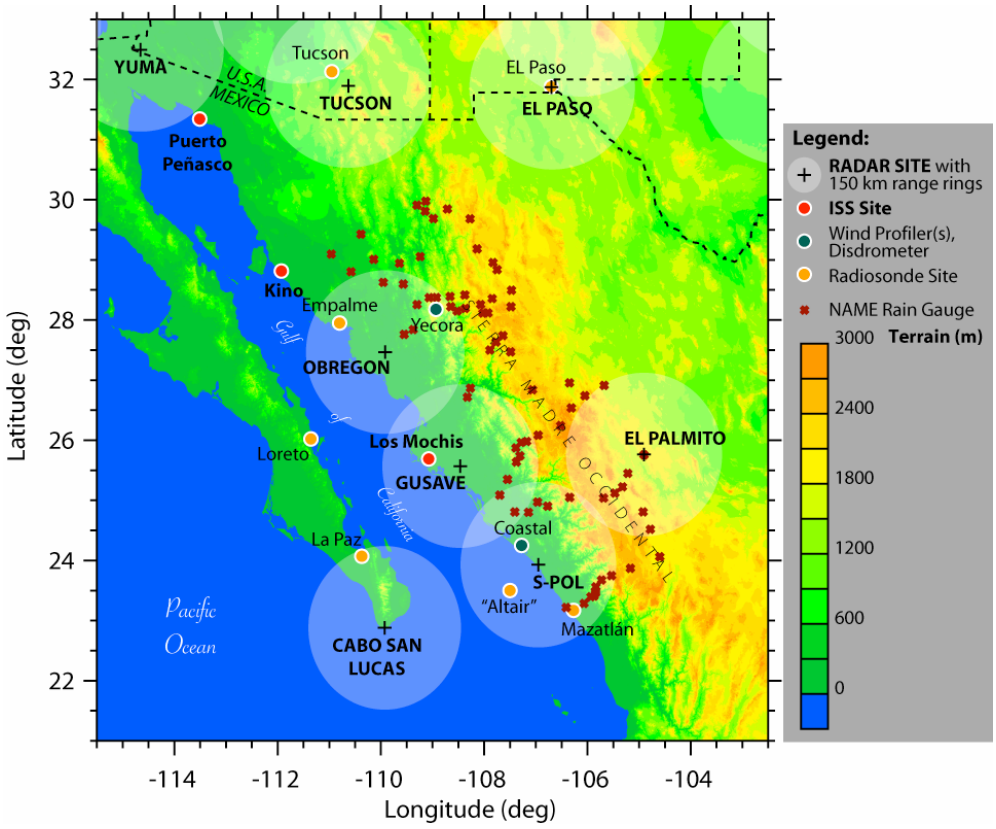

Figure 1. Locations of radars and other instrument sites during NAME 2004. Plot courtesy of NAME community.

The Version 2 composites cover the period 7/8 0000 UTC thru 8/21 2345 UTC. The temporal resolution is 15 minutes. Significant gaps in radar coverage occurred during this time – too many to enumerate. Refer to the composite files themselves to determine the availability of composites and/or individual radars.

2.0 INSTRUMENT DESCRIPTION

Meteorological Radars

S-Pol: S-band, Doppler, polarimetric (linear H & V polarizations), 1.0° beamwidth
Cabo: C-band, Doppler, 1.4° beamwidth

Guasave: C-band, Doppler, 1.4° beamwidth

3.0 DATA COLLECTION AND PROCESSING

INTRODUCTION

Prior to creation of the 2-D composites, all NAME radar data were subjected to vigorous quality control efforts. There were three radars available during the NAME EOP: S-Pol, Guasave, and Cabo. We will subdivide the discussion of these efforts by radar.

S-POL

S-Pol is an S-band polarimetric Doppler radar that was located near La Cruz in Sinaloa. It was available 7/8-8/21 during 2004. Version 2 composites contain data from 7/8 onward.

The S-Pol radar was run at two main PRFs, 720 Hz and 960 Hz. 720 Hz was the most common and provided an unambiguous range of ~210 km. 960 Hz was less common and provided a range near 150 km. Some other PRFs were used occasionally, especially early in the NAME EOP. These ranged between 720 and 1000 Hz.

Reflectivity (Z_H) and differential reflectivity (Z_{DR}) calibration biases were corrected by NCAR/EOL prior to any further QC efforts.

Due to the availability of polarimetric variables, we were able to automate most of the quality control for S-Pol. The goal was to eliminate clutter/AP, noise, second-trip echo, and insect echo. In order to accomplish this, the following filters were applied to all 360° PPI sweeps at 0.8 and 1.3° elevation (note, before 7/10 data were taken at 0.5 and 1.0°, so substitute these numbers in the following discussion when considering early EOP S-Pol data):

ρ_{HV} – Range-based filter. We removed data with correlation coefficient (ρ_{HV}) < 0.8, except for range > 90 km and Z_H > 20 dBZ. For those data, we only eliminated gates with ρ_{HV} < 0.5 (noise/clutter).
SD(Φ_{DP}) – We calculated standard deviation of differential phase, SD(Φ_{DP}), over a moving window of 11 gates (1.65 km) and eliminated any data where SD > 18° if Z_H > 35 dBZ. If Z_H < 35 dBZ, we eliminated data where SD > 10° (noise/clutter).
LDR/Φ_{DP} – We eliminated data where linear depolarization ratio (LDR) > –5.0 and Φ_{DP} > 30° (second-trip).
Z_H/Z_{DR} – We eliminated all data where Z_H < 0 dBZ. For Z_H between 0 and 10 dBZ, we eliminated data where Z_{DR} > 1 dB. For Z_H between 10 and 35 dBZ, we eliminated data where $Z_{DR} > 1+0.075*Z_H$ (noise/insects).

The S-Pol test pulse was removed in an automated matter by eliminating the last several gates where it was usually located. This position varied with PRF. Occasionally, the test pulse was located elsewhere, and had to be removed by hand using soloii.

Φ_{DP} was filtered using a 21-gate (3.15-km) finite impulse response filter developed by John Hubbert of NCAR and V. N. Bringi of Colorado State University. Small data gaps within this moving window were filled using linear interpolation, in order to increase the amount of useable windows for subsequent specific differential phase (K_{DP}) calculation. K_{DP} was calculated from the slope of a line fitted to the filtered Φ_{DP} field. The window over which this line was fitted changed depending on the Z_H of the central gate. If Z_H < 35 dBZ, then we fitted to 31 gates (4.65 km). For Z_H between 35 and 45 dBZ, we fitted to 21 gates (3.15 km). For Z_H > 45 dBZ, we fitted to 11 gates (1.65 km). This allowed for more accurate K_{DP} estimates at both high and low Z_H. For a handful of sweeps during a major storm on 8/3, we found that Φ_{DP} became folded due to the large areas of intense rain. Prior to filtering and K_{DP} estimation, we unfolded the Φ_{DP} field by hand using soloii.

Z_H and Z_{DR} were corrected for differential attenuation based on examining the behavior of these variables as a function of Φ_{DP} for a given range of K_{DP} values. In this situation, we found that both Z_H and Z_{DR} decreased with increasing phase shift, due to attenuation by liquid water. Lines were fitted to these relationships, and the slopes were used to correct Z_H and Z_{DR} as Φ_{DP} increased above 0°. An example for Z_H is shown in Fig. 2. The coefficient (slope) used for Z_H was 0.0171 dBZ $^{\circ -1}$. The Z_{DR}-Φ_{DP} relationship was noisy. The fitted slope was 0.0048 dB $^{\circ -1}$, but due to the scatter in this relationship, we used the Z_{DR} correction coefficient from the TRMM-LBA project in 1999, which was 0.0042. For 100° of phase shift (common in strong MCS convection), we would correct Z_H by +1.71 dBZ and Z_{DR} by +0.42 dB.

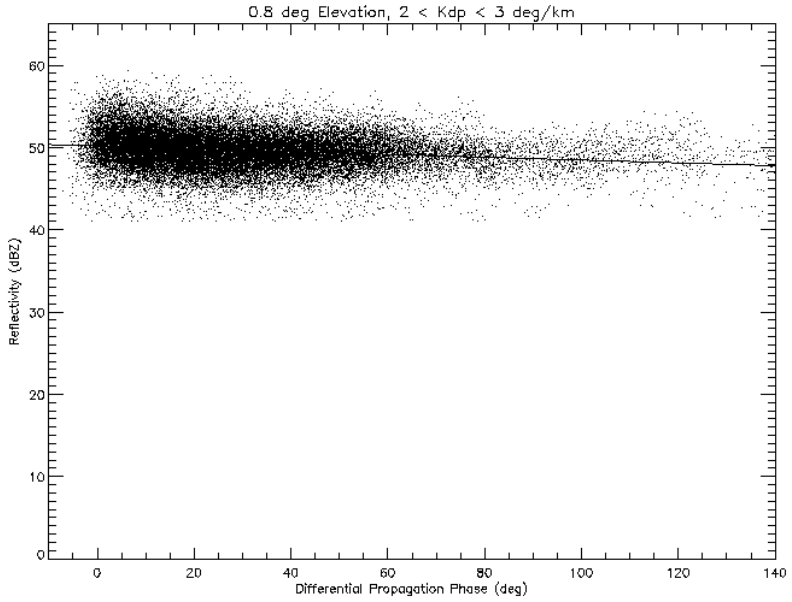

Figure 2. Scatterplot of Z_H vs. filtered Φ_{DP} for the specified K_{DP} range, using one week of S-Pol data from NAME. Also shown is the linear fit to the data.

Z_H was further corrected for gaseous attenuation. We used the established value of 0.007 dBZ km^{-1} (Battan 1973). This has to be doubled for a given range since the radar beam travels to and from the target. The correction at 200 km is +2.8 dBZ.

Despite all the thresholds, some clutter and insect echo remained after automated filtering. These remaining spurious echoes were subsequently removed by hand with soloii. In addition, we despeckled the data using the soloii algorithm. This removed any echo that contained only 2 or fewer contiguous gates.

Figure 3 shows an example of the beam blockage observed at S-Pol during NAME 2004. Significant amounts of beam blockage occurred in S-Pol's NE sector (351-105° azimuth). This blockage was caused by mountain peaks intercepting the radar beam at low elevation angles. The location of the blocks was determined to the nearest degree in azimuth and nearest km in range by visual inspection of clear-air radar sweeps. Then, within rainfall (identified by the CSU hydrometeor identification or HID algorithm; Tessendorf et al. 2005) in the blocked regions, we examined the behavior of Z_H as a function of azimuth for a given K_{DP} range. Because there were sometimes multiple blocks along the same ray, we had to do this analysis for both exterior (Fig. 4) and interior (Fig. 5) ranges, the values of which varied as functions of azimuth and reflected the locations of the blocks. However, we never examined data within 20 km of S-Pol. Due to the self-consistency between polarimetric variables, for a given range of K_{DP}, Z_H should vary only over a small range as well. If Z_H drops significantly below this range, that signals a block. The difference in the median Z_H values in unblocked regions, and median Z_H values in a blocked ray, is the +dBZ correction that needs to be applied to Z_H.

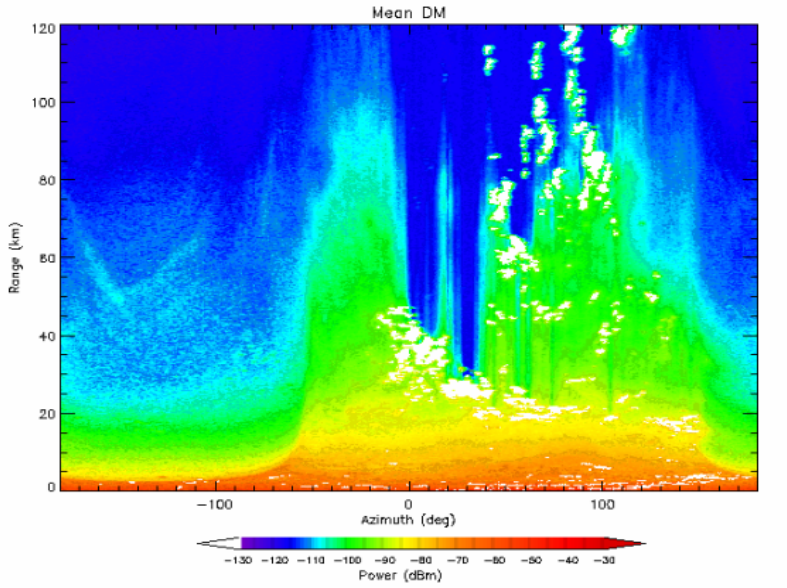

Figure 3. Average power return for 12 h of clear air returns at S-Pol. Blocks show up as significant reductions in mean power in the azimuths -9° (351°) to 105°. Clutter is flagged in white. Note that there were sometimes multiple blocks along the same ray.

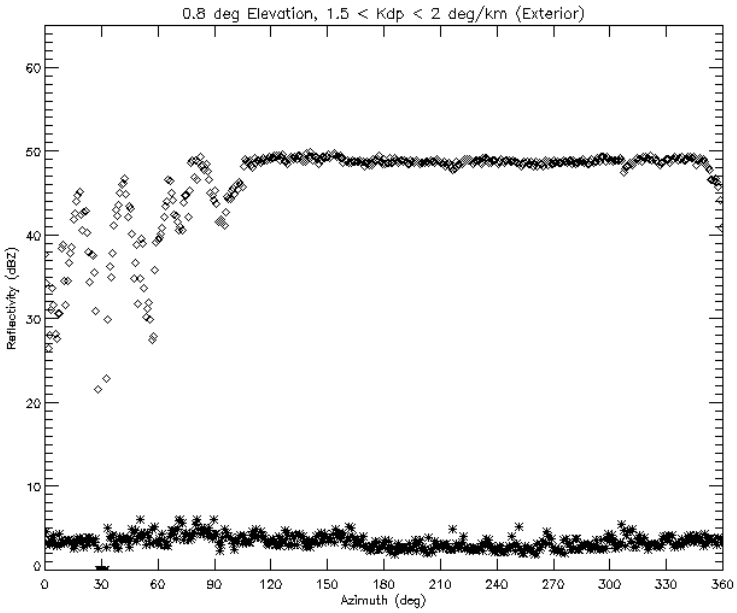

Figure 4. Median Z_H in rain as a function of azimuth for the indicated elevation and K_{DP} range (diamonds). Also shown is standard deviation in Z_H (*). This plot used S-Pol data throughout the NAME EOP and is for exterior ranges.

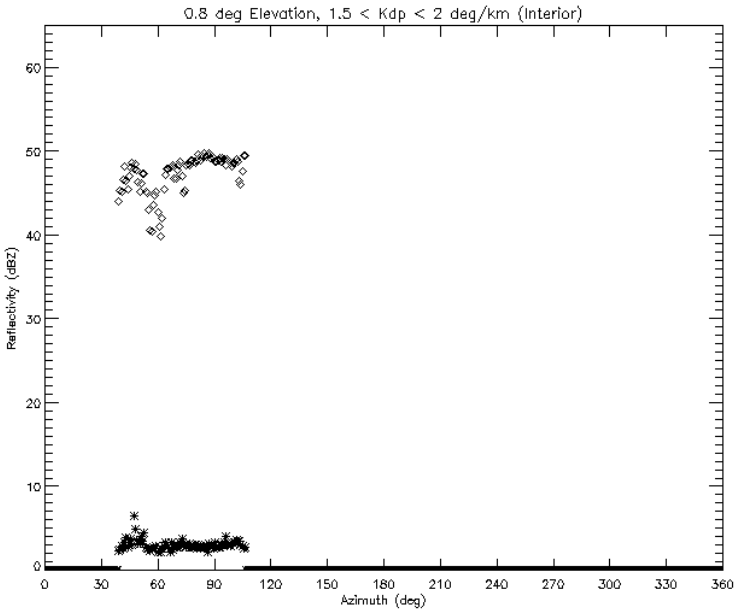

Figure 5. Median Z_H in rain as a function of azimuth for the indicated elevation and K_{DP} range (diamonds). Also shown is standard deviation in Z_H (*). This plot used S-Pol data throughout the NAME EOP and is for interior ranges. Note that interior blocks only existed at a subset of angles.

However, in major blocks near 30° and 56° there was near total signal loss at 0.8°. Here, we used information from 1.3° at all ranges greater than that of the block. In addition, we filled in low-level gaps caused by clutter removal (at 0.8° elevation) using information from higher sweeps (1.3°). QC flags reflecting the elevation angle used at a particular

gate in the blocked azimuths were created, and are reflected in the height_MSL field in the final regional composites.

We performed limited intercomparisons of corrected S-Pol Z_H with TRMM satellite overpasses. Figure 6 shows an example of this intercomparison. S-Pol data were interpolated to the same horizontal grid as the native TRMM Precipitation Radar (PR) data. The quality-controlled PPI sweeps closest in time (within 1-2 minutes) to the overpass was chosen. To make an estimate of reflectivity at each gridpoint, it was required that at least 8 ground radar gates had meteorological data and were within 5 km horizontally and 250 m vertically of the PR gridpoint location. There is a high variance in the distribution of PR-GND Z values, which is expected given the radically different radar types, beam and scan geometries, etc. But the mean value of corrected S-Pol Z_H data is within 0.06 dBZ of TRMM PR, suggesting that the blockage correction (along with other reflectivity corrections; e.g., for attenuation) did an excellent job.

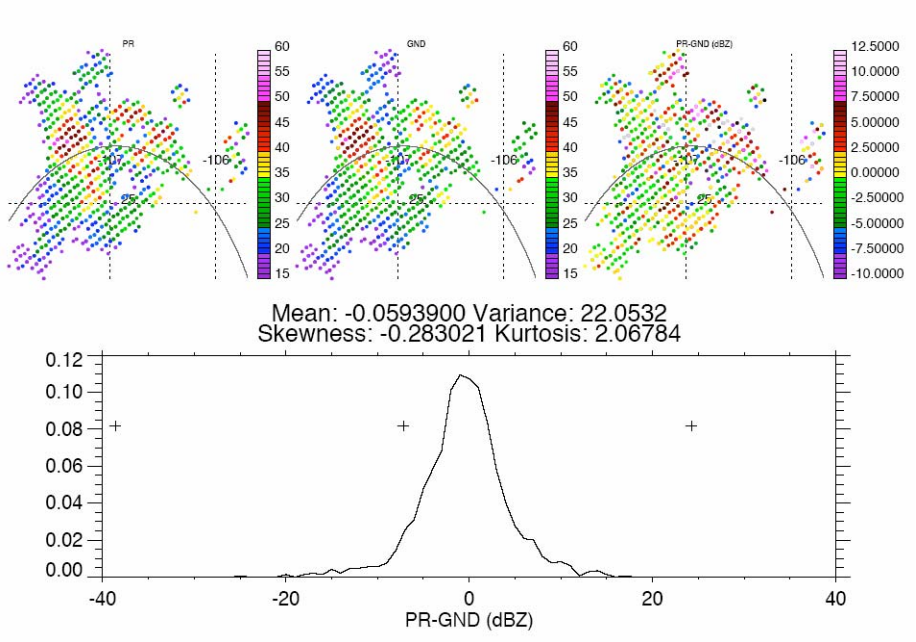

Figure 6. Maps of TRMM PR, corrected S-Pol (GND), and PR-GND Z_H values, along with a distribution of PR-GND, for a single TRMM overpass. The curve in the maps is an S-Pol range ring, indicating the radar was roughly SSW of the map center. The NE sector of S-Pol, corresponding to the eastern portions of the maps, was affected by beam blockage.

We corrected blocked Z_{DR} at 0.8° and 1.3° using the methodology of Giangrande and Ryzhkov (2005). Here we examine Z_{DR} variability in drizzle (as defined by the CSU HID algorithm) as a function of azimuth. Figure 7 shows an example for exterior ranges.

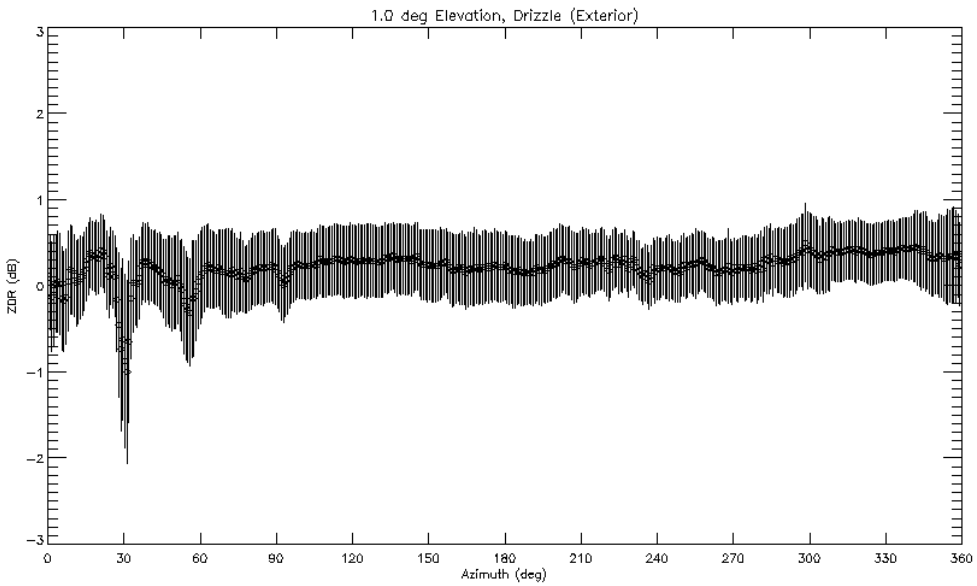

Figure 7. Median Z_{DR} in drizzle as a function of azimuth for the indicated elevation (require KDP < 0.1; diamonds). Also shown is standard deviation in Z_{DR} (error bars). This plot used S-Pol data throughout the NAME EOP and is for exterior ranges.

Rain rates were calculated using a modified version of the CSU blended rainfall algorithm (Cifelli et al. 2002). This algorithm varies between $R(K_{DP})$, $R(Z_H,Z_{DR})$, $R(Z_H)$, and $R(K_{DP},Z_{DR})$ depending on the values of the polarimetric variables and the presence of mixed-phase precipitation. It has been demonstrated to provide superior rain estimates to Z-R or any other polarimetric rain estimator alone. The decision tree used by this algorithm is shown in Fig. 8.

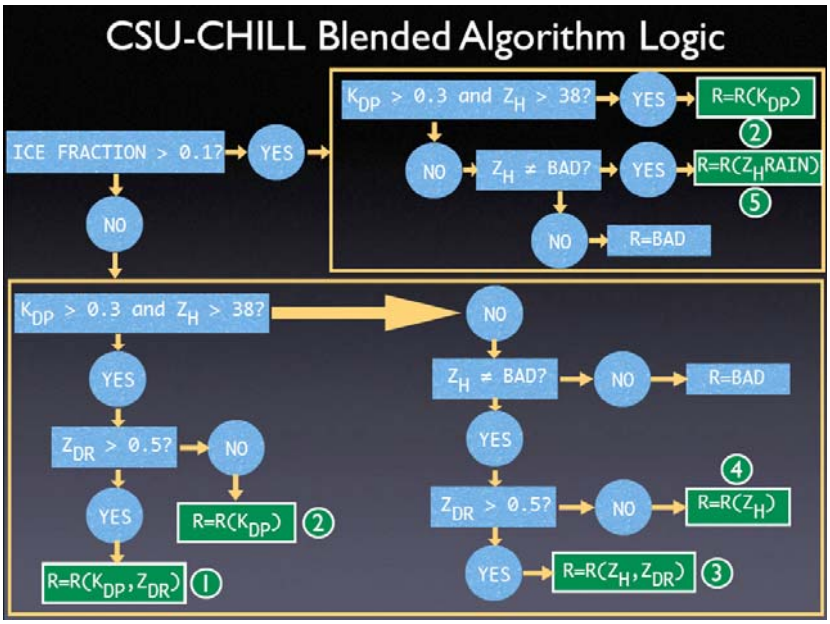

Figure 8. Decision tree for CSU blended rainfall algorithm, used with S-Pol data from NAME. Figure courtesy of Dr. Rob Cifelli of CSU.

The modifications were as follows:

1) K_{DP}-based rain estimates were not used if K_{DP} did not fall within the expected range of behavior, which depends on the corresponding Z_H value. This occurred even if all other conditions for $R(K_{DP})$ or $R(K_{DP},Z_{DR})$ were met.

2) The Z-R used was $Z=133R^{1.5}$, which was determined via the polarimetric tuning methodology of Bringi et al. (2004). For one week's S-Pol data, we averaged the Z-R coefficients obtained for all viable gates using this methodology, to arrive at the final relationship. Intercomparisons with gage rain rates at the NOAA profiler site NW of S-Pol found that this Z-R minimized normalized mean error (71.6%) and bias (+30.9%) with this particular gage, even compared to fits developed from linear regression. The Z-R was capped at 57 dBZ to minimize ice contamination. Note that, in regions with significant amounts of mixed-phase precipitation, usually we were using other polarimetric rain estimators, especially $R(K_{DP})$, not a Z-R.

3) The maximum rain rate allowed was 250 mm h^{-1}, which is the R associated with Z=57 dBZ. If $R > R_{max}$ (no matter what the final method used to estimate R was), then R was set to R_{max}.

GUASAVE

Guasave is a C-band Doppler radar operated by the Mexican weather service (SMN). It was available 6/10-8/31+, but we have only processed data for the S-Pol deployment (7/8-8/21). Due to a recording problem, Guasave data are not available for most of the time period 7/23-7/31. Guasave was operated at a number of different PRF and calibration settings, and only one elevation angle (which changed between 0.5, 1.0, and 1.5° throughout the project). For the most part, the PRF remained pretty low (shortest max range > 200 km), so the Doppler data have a lot of folds. We never addressed the QC of the velocity data, only reflectivity.

Because Guasave ran at only one sweep angle, there were updates every minute or so. We only used the most complete sweep closest in time to each 15-minute mark (##:00, ##:15, ##:30, and ##:45). This usually meant the sweep was within 0-2 minutes of this mark.

Quality control was half-automated, half-not. We applied automated filters on Z_H, Z_H and noise-corrected power (NCP; usually NCP is sufficient alone but the low PRF required an additional filter on Z_H to avoid deleting turbulent convective cores), and on total power (DM). The value of these filters changed as calibration offsets changed. The specific values were determined by visual inspection of its associated time period. After filtering was performed, we despeckled the data using the same methodology as S-Pol despeckling. These automated procedures removed most of the noise.

Due to antenna backlash (a lag between radar gears, servo mechanism, and encoders that manifests as an offset between azimuths obtained during clockwise and counter-clockwise motion of the antenna), Guasave required a correction to measured azimuths.

The correction applied depended on the rotation direction of the antenna (which changed every few days) and the azimuthal spacing of the beams (which changed occasionally when calibration settings changed). The correction varied between +/– 0.42 and 0.63°.

We then applied an automated clutter filter. This clutter filter queried a clutter map created from clear-air Guasave sweeps taken over several days. Due to different PRFs, elevation angles, and pulse lengths, we had separate clutter maps for July and for August Guasave data. For each gate in every ray, we queried the clutter map to see if clutter occupied that position. If so, the data were removed. There was a lot of clutter at Guasave; so many gaps will appear in storms that overran the clutter, which was a common occurrence.

We hand edited the filtered dataset for any remaining clutter, noise, second-trip, and insects using soloii. Often, there were strong insect echoes overnight at Guasave. These sometimes could have been mixed in with small rain echoes. In such situations, it was basically impossible to tell whether the echo was insects or precipitation, and we usually deleted the echo, in order to avoid contamination of rain rates by insect echoes. Thus, many times there may be missing echo despite the occurrence of small rain storms, especially close to Guasave (within ~60 km). However, we managed to preserve stronger and larger storms, which were more easily identified when embedded within insect echo.

A reflectivity offset was then applied to the data based on visual and statistical intercomparisons with S-Pol reflectivity. The statistical evaluation compared the closest gates within 500 m horizontal and 200 m vertical. Histograms of reflectivity differences were obtained from this statistical intercomparison. In addition, visual intercomparison of well-placed echoes was done using soloii. Based on both these methods, a reflectivity correction was applied to the SMN radar data. The value of this correction depended on the particular setting of Guasave, which varied throughout the NAME EOP. Typically, several days would pass and a new setting occurred due to an engineer working on the radar. No gradual drift in calibration was observed, only step-wise changes as described above. This was confirmed by examining time series of noise reflectivity at a specific range. Occasionally, a calibration change lasted only a few hours, or even only one sweep. These often did not lend themselves well to intercomparison with S-Pol, due to the meteorological situation. Under these circumstances, visual and statistical intercomparisons were made with Guasave sweeps immediately prior to and after the time of the "rogue" setting. In addition, we examined noise reflectivity to identify rogue settings that were similar in terms of offset.

Attenuation correction by rain was based on the GATE algorithm (Patterson et al. 1979), which iteratively corrects Z_H at a gate based on the theoretical treatment of attenuation by all the rainfall up to the given gate. The potential correction was capped at +8 dBZ, but for C-band is usually on the order of +2-3 dBZ downrange of significant convection.

Z_H was further corrected for gaseous attenuation. We used the established value (at C-band) of 0.008 dBZ km^{-1}. (This has to be doubled for a given range since the radar beam travels to and from the target.) The correction at 200 km is +3.2 dBZ.

The value of the final applied Z_H offset for Guasave varied from +6 dBZ to –7 dBZ. The attenuation-corrected Guasave data were compared to the attenuation-corrected S-Pol data to confirm all the applied offsets. We believe that final, corrected Guasave Z_H measurements are accurate to within 1-2 dBZ. Accuracy could be even better than this (within ~0.5 dBZ), as shown by the TRMM intercomparison in Fig. 9. Due to sensitivity issues, at long ranges (> 150 km) Guasave had difficulty detecting below 20 dBZ. At closer ranges, Guasave could detect down to ~10 dBZ.

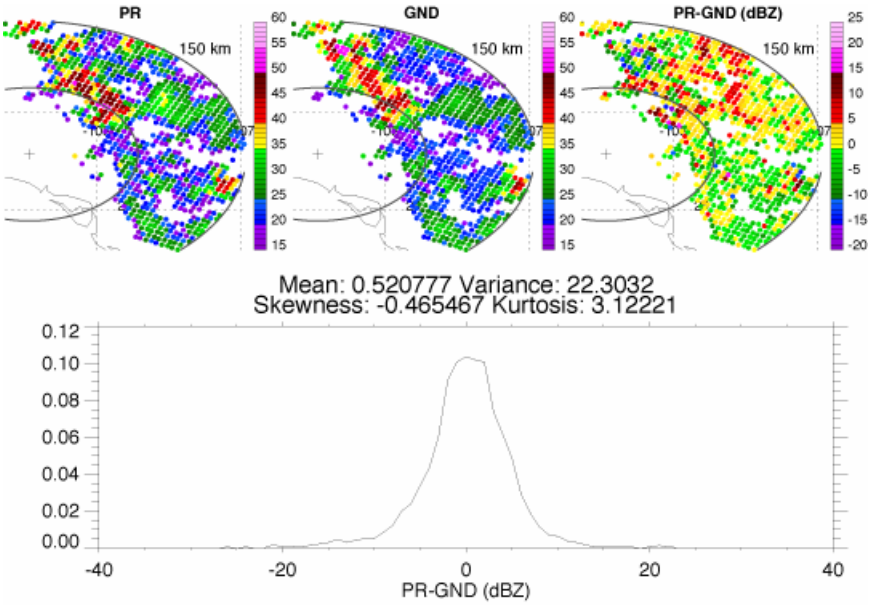

Figure 9. Maps of TRMM PR, corrected Guasave (GND), and PR-GND Z_H values, along with a distribution of PR-GND, for a single TRMM overpass. The curves in the maps are Guasave range rings, with the crosshairs showing the radar location.

Guasave did not appear to have many blocks. However, at low angles in July, Z_H values near 25° azimuth could be partially blocked. Blockage was nowhere near as big a problem as at S-Pol, and no correction for blockage was attempted.

Rainfall rates were determined from the aforementioned Z-R relationship, with capping at 57 dBZ (250 mm h^{-1}) to minimize ice contamination.

CABO

Cabo is a C-band Doppler radar operated by the Mexican weather service (SMN). It was available 7/16-8/31+, but we have only processed data for most of the S-Pol deployment (7/16-8/14). Data after 8/14 were unrecoverable due to a disk error. The QC process and results for Cabo were very similar to those of Guasave, with the following changes:

1) Cabo only ran at a single elevation angle, 0.6°.

2) Cabo never had major storms overpassing its clutter, so hand-removal of clutter was all that was required. No clutter map was needed.

3) Final Z_H offsets varied between 0 and +6 dBZ.

4) Cabo was partially blocked by terrain between 300 and 60° azimuth. However, most storms remained outside this region. No blockage correction was attempted.

5) Cabo did not require any azimuth correction.

6) Cabo had persistent sea clutter to the south and west. This was indistinguishable from regular precipitation because we lacked upper elevation info, and the echo had coherent Doppler signatures. An intercomparison between v1 reflectivity composites and GOES IR brightness temperatures (T_B) on the same grid revealed that most sea clutter clustered above 290 K (Fig. 10), and these echo temperatures were confined almost exclusively to the Cabo region. We have not deleted this echo, to allow for uncertainty and the ability to do sensitivity studies, but in the v2 composites *we recommend as a first step that users exclude any echo with T_B > 290 K.*

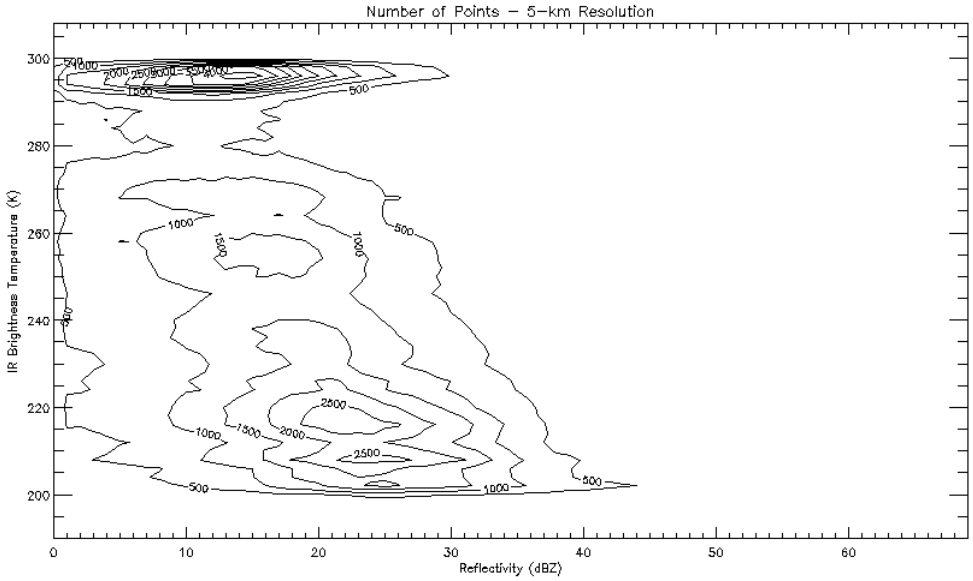

Figure 10. Density contours for number of points with specific Z_H and T_B values, for the entire version 1 dataset at 0.05° resolution (~5 km). The sea clutter clusters above 290 K, with real precipitation at colder temperatures.

CHANGES FROM VERSION 1

1) The range over which SD(Φ_{DP}) was calculated in S-Pol data was shortened by 10 gates in order to reduce the influence of noise near cell edges.

2) The Z_H/Z_{DR} insect filter was made more stringent in S-Pol data.

3) The requirement on the size of gaps to be filled in S-Pol Φ_{DP} data were made more stringent. The net effect was that K_{DP} was calculated only over a smaller portion of cells, in order to reduce noisiness in this variable.

4) Due to reduced noisiness in K_{DP}, and developing the correction only using gates identified as rain by the S-Pol hydrometeor identification algorithm, beam blockage correction at S-Pol is much improved, with 0.8° elevation corrected in

nearly all rays, with less reliance on the 1.3° sweep, and no usage of 1.8. Z_{DR} is now corrected as well.

5) We used a different Z-R relationship, one developed from polarimetric tuning. This, in addition to greater reliance in the S-Pol rain algorithm on corrected Z_{DR} in blocked regions, significantly brought down rain rates, matching better with the NERN gages when comparing v2 to v1 (Fig. 11). There is still a high bias near the northern end of the v2 composites. We suspect this is due to ice contamination at long ranges from Guasave.

6) IR brightness temperature from GOES (T_B) was added to the gridded dataset, among other things to help identify sea clutter near Cabo. See the improvement near Cabo from v2 to v1 in Fig. 11 when excluding echo with $T_B > 290$ K.

7) 0.01° composites are no longer offered.

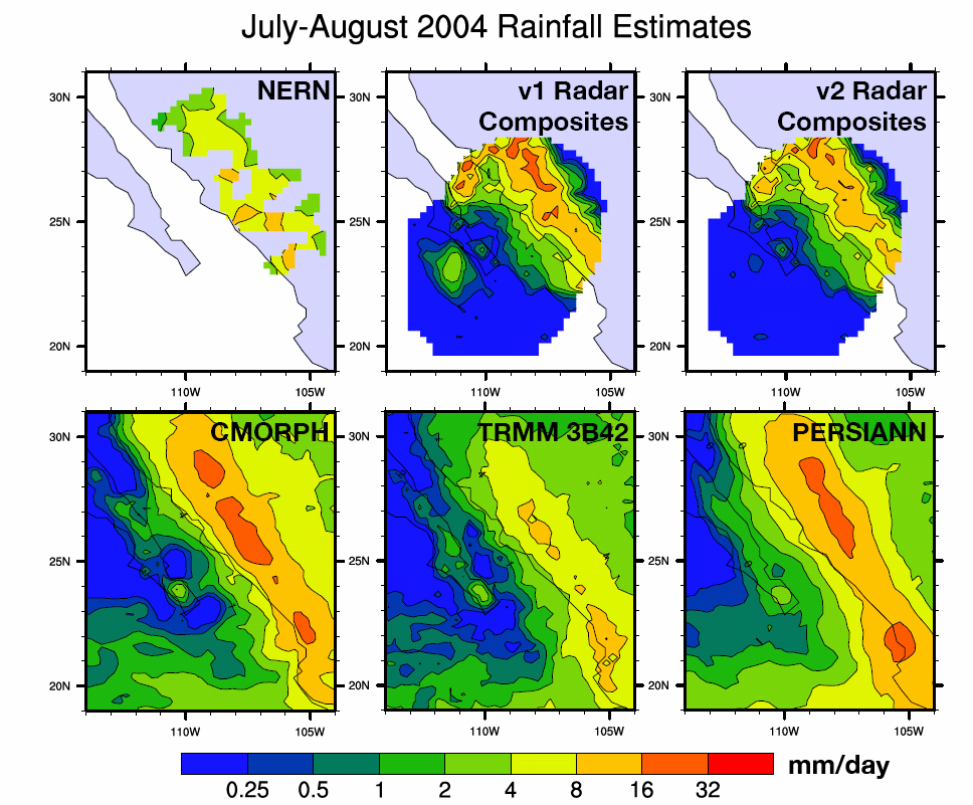

Figure 11. **July-August 2004 rainfall from several different estimation methodologies.**

PLANS FOR VERSION 3

1. We will create a merged radar-gage rainfall product, similar to the Stage IV rainfall products NOAA creates for the United States.

2. We *may* change S-Pol data filtering by basing it off fuzzy-logic particle identification, which can identify insects, clutter, etc. without the use of fixed thresholds.

Version 3 of the regional composites will be available by summer 2007. That will be the final version of the NAME regional radar composites.

4.0 DATA FORMAT

INTRODUCTION

These two-dimensional composites were produced on a cylindrical projection (lat/lon) grid every 15 minutes from up to three radars situated near the mouth of the Gulf of California in summer 2004. Four fields were created:

- height_MSL (radar gate height in meters above mean sea level)
- DZ (reflectivity in dBZ)
- RR (rainfall rate in mm h^{-1})
- TBR (GOES IR brightness temperature T_B in Kelvin)

We also provide topographic DEMs for each grid resolution provided, as separate files, so users can determine height AGL from the height_MSL field.

A missing_value was assigned to grid points in regions not covered by radar.

- height_MSL.missing_value: –32768
- DZ.missing_value: –32768
- RR.missing_value: –32768
- TBR.missing_value: –32768

Where no precipitation echo was present, but the grid point was covered by radar, these values were assigned:

- DZ not missing, but no precipitation echo: –Inf
- RR not missing, but no rainfall: 0.0

height_MSL should be present at all points covered by radar. TBR should be present at all points in the domain.

Filenames also denote the UTC dates and times for which the composites are valid. The format of the filenames is cYYYYMMDD_HHmmSS_dkm.nc where YYYY is the four-digit year, MM is the two-digit month, DD is the two-digit day, HH is the two-digit hour, mm is the two-digit minute, SS is the two-digit second, and d is a 2 or a 5, depending on whether a 0.02° grid or a 0.05° lat/lon grid was used. 0.02° is about 2 km and 0.05° is about 5 km.

PREPROCESSING

Before converting to a lat/lon grid, the data along each ray were smoothed and resampled to a sparser array. Logarithmic fields (such as DZ) were linearized first. The moving average window applied along the range dimension was approximately 1000 m wide; i.e., gate_smoother = LONG(1000/r), where gate_smoother was the width of the window in

gates, LONG(x) was the greatest integer <= x function, and r was the original gate spacing in meters. After smoothing, the data were resampled every gate_smoother gates, producing a new gate spacing (or newCell_Spacing) of newCell_Spacing = r*gate_smoother, where r was the same as above. The gate_smoother and newCell_Spacing variables were both saved in the composite netCDF file.

COMPOSITING METHODOLOGY

Data from individual radars were converted from radar-centric spherical coordinates to an earth-centric lat/lon/height grid. The spherical radar coordinates of azimuth, elevation angle, and range were transformed to latitude, longitude and height with the following formulas.

First of all, azimuth was zero at due north and increased clockwise. Elevation angle was zero at the horizontal and increased upward. Slant range was zero at the radar and increased with distance along the radar beam.

Given an array of gates from an individual radar beam, the slant range to the center of each gate was found with this simple formula:

```
slant_range = distance_to_first_gate+Gate_Spacing*(Gate_index+0.5)
```

where Gate_index is an integer beginning at 0.

Then using the 4/3 effective Earth radius model following Eqns. 2.28b and 2.28c of Doviak and Zrnic (1993), we calculate height above MSL and great circle distance:

```
height_MSL = SQRT(slant_range^2 + (ke*R)^2 +
      2*slant_range*ke*R*sin(elevation)) - ke*R + Altitude

sfc_range = ke*R*asin(slant_range*cos(elevation)/(ke*R+height_MSL))
```

where ke = 4/3, R is earth radius (6371 km), and altitude is the radar height.

From sfc_range, we compute latitude and longitude of each gate, given the original radar coordinates (lat1,lon1):

```
lats = asin( sin(lat1)*cos(sfc_range/R) +
      cos(lat1)*sin(sfc_range/R)*cos(azimuth) )
lons = lon1+asin(sin(azimuth)*sin(sfc_range/R)/cos(lats))
```

Consecutive radar rays from approximately the same elevation angle were grouped into individual sweep files. Sweep files from about the same time and the lowest elevation angle were combined every 15 minutes to produce network composites.

This is how the sweep files were combined. Where radar gates overlapped, the lowest gate took precedence and higher gates were eliminated. Note that this did not necessarily preserve the highest reflectivity gate in a vertical column. However, since reflectivity usually decreases with height, this was generally the case. Future versions of the composite dataset may include such a field based on the highest reflectivity found in a vertical column, but there are not expected to be large differences. An overlap occurred

wherever a gate from one radar was within one half-gate width and one half-beam width of a gate from another radar.

After eliminating higher gates from overlapping sections, the remaining gates were combined and interpolated to a regular lat/lon grid. The actual software was written in IDL and used a combination of QHULL (which formed the Delauney triangulation of points on the surface of a sphere) and GRIDDATA, which used the triangulation results to produce a regular grid. For more information on Delauney triangles, QHULL, and GRIDDATA used by IDL see Barber et al. (1996). Also see http://www.qhull.org/ and http://www.rsinc.com/idl/pdfs/quickref.pdf.

An inverse-distance weighting method was employed to produce the interpolated values using only gates within 0.03° of each gridpoint. A circular smoothing filter with a radius of 0.001° was also applied. The actual IDL commands used to produce the gridded data were

```
QHULL, lons, lats, triangles, SPHERE=s

gridded_data = GRIDDATA(lons, lats, data, triangles=triangles, /DEGREES,
      /SPHERE, /Inverse_Distance, /GRID, XOUT=grid_lons, YOUT=grid_lats,
      max_per_sector=5, MIN_POINTS=3, SEARCH_ELLIPSE=0.04, SMOOTHING=0.,
      MISSING=-32768.)
```

where grid_lons and grid_lats were the longitudes and latitudes of the grid columns and rows.

The first row of the gridded array (going from south to north) was at 19.8 N and the last row at 28.9 N. The first column (west to east) was at –113.1 E and the last at –104.8 E.

From the IDL code:

```
limit = [19.8, -113.1, 28.9, -104.8]
dlon = limit[3] - limit[1]
dlat = limit[2] - limit[0]
grid_lons = limit[1] + FINDGEN(ROUND(dlon/latlon_spacing) + 1) *
      latlon_spacing
grid_lats = limit[0] + FINDGEN(ROUND(dlat/latlon_spacing) + 1) *
      latlon_spacing
```

Grid_spacing	final gridded array size (longitude x latitude pts)
0.05°	167 x 183
0.02°	416 x 456

Several additional fields associated with the original component sweep files, such as elevation angle, starting time, and radar coordinates were preserved with the composite netCDF file under the iradar dimension. The first index of the iradar dimension holds values associated with SPOL, the second index holds values associated with CABO, and the third with the GUASAVE radar.

Output format: netCDF

For more info about netCDF and related software, see http://my.unidata.ucar.edu/content/software/netcdf.

Here is an example header dump using ncdump:

```
netcdf c20040806_0200_2km {
dimensions:
      time = UNLIMITED ; // (1 currently)
      latitude = 456 ;
      longitude = 416 ;
variables:
      float DZ(time, latitude, longitude) ;
            DZ:_FillValue = -32768.f ;
            DZ:missing_value = -32768.f ;
            DZ:long_name = "reflectivity" ;
            DZ:units = "dBZ" ;
      float RR(time, latitude, longitude) ;
            RR:_FillValue = -32768.f ;
            RR:missing_value = -32768.f ;
            RR:long_name = "rainfall rate" ;
            RR:units = "mm/h" ;
            RR:valid_min = 0.f ;
      float TBR(time, latitude, longitude) ;
            TBR:_FillValue = 330.f ;
            TBR:units = "K" ;
            TBR:valid_min = 0.f ;
      float height_MSL(time, latitude, longitude) ;
            height_MSL:_FillValue = -32768.f ;
            height_MSL:missing_value = -32768.f ;
            height_MSL:units = "meters" ;
            height_MSL:long_name = "height above mean sea level" ;
      float latitude(latitude) ;
            latitude:units = "degrees_north" ;
            latitude:valid_range = -90.f, 90.f ;
      float longitude(longitude) ;
            longitude:units = "degrees_east" ;
      int time(time) ;
            time:units = "seconds since 1970-01-01 00:00 +0" ;

// global attributes:
            :spol_ncfile =
      "/data1a/pd/ahijevyc/NAME/2.0/ncswp_SPOL_20040806_015959_COMPOSITE
      .nc" ;
            :cabo_ncfile = "missing" ;
            :guas_ncfile =
      "/data1a/pd/ahijevyc/NAME/2.0/ncswp_GUASAVE_20040806_020002.320_u1
      _s201_1.5_PPI_.nc" ;
            :history = "Wed Feb 28 11:33:52 2007: ncatted -a
      version,global,o,c,2.0 -O c20040806_0200_2km.nc\n",
                  "Wed May 31 14:22:17 2006: ncks -v
      TBR,RR,DZ,height_MSL -O ./c20040806_0200_2km.nc
      ./c20040806_0200_2km.nc\n",
                  "Tue May 23 11:50:51 2006: ncrename -v
      base_time,swpbase_time -v RR45300,RR -v DZ45300,DZ -v
      height_MSL45300,height_MSL -O c20040806_0200_2km.nc\n",
                  "Tue May 23 11:50:51 2006: ncks -O -a -x -v
      volume_start_time,Nyquist_Velocity,Radar_Constant,rcvr_gain,ant_ga
      in,sys_gain,bm_width,pulse_width,band_width,peak_pwr,xmtr_pwr,nois
      e_pwr,tst_pls_pwr,tst_pls_rng0,tst_pls_rng1 c20040806_0200_2km.nc
      c20040806_0200_2km.nc\n",
                  "Created Tue May 23 11:49:21 2006 with IDL" ;
```

```
            :IDL_VERSION_ARCH = "x86" ;
            :IDL_VERSION_OS = "linux" ;
            :IDL_VERSION_RELEASE = "6.2" ;
            :latlon_spacing = "0.02" ;
            :version = "2.0" ;
            :contact = "David Ahijevych" ;
            :email = "ahijevyc@ucar.edu" ;
            :address = "National Center for Atmospheric Research\\nP.O.
      Box 3000\\nBoulder, CO, 80307" ;
            :nco_openmp_thread_number = 1 ;
}
```

Note how present/missing radars are classified by the spol_ncfile, cabo_ncfile, and guas_ncfile variables. Use this information to identify which radars are available within a specific composite file.

Changes for version 2.1 since version 2.0

When version 2.0 was released, the netCDF file had a global attribute named “version” that was mistakenly left at “1.0”, instead being set to “2.0”. This has been fixed. Now the attribute is either set to “2.0” or “2.1”, depending on whether additional changes were made. Some network composites were completely reconstructed using a wider time window. For these files, the "version" was changed from “2.0” to "2.1". Both versions (2.0 and 2.1) are mixed into the same monthly tar file with "2.1" in its filename.

The new time constraint is now explained. To fill in dozens of missing sweeps, the temporal window was widened from 7 to 17 minutes on either side of the nominal time. The nominal time was always a multiple of fifteen minutes. As before, if there were multiple sweeps from an individual radar within a time window, the sweep closest to the nominal time was used in the composite. This meant a sweep could be used for up to three consecutive network composites. This allowed us to fill in dozens of missing sweeps without making the time window unreasonably wide. 354 out of the total 4308 composites (8%) were affected by this relaxed time constraint. Prior to this fix, the Guasave sweep would often flicker in and out of the composite (see 21 July, 2004). This was due to a hard disk failure that corrupted many Guasave files. But after the change, the radar loops and accompanying Hovmoller plots are much smoother. You notice this effect when you loop the composites. One section of the composite might be static for a frame or two while the pixels surrounding an adjacent radar continue to change.

Changed the "time" variable in the netCDF file to the nearest multiple of 15 minutes. This is the nominal time, or the time listed in the filename. Before, the time variable was taken from one of the radar sweeps, which was not necessarily a multiple of 15 minutes. It was close, but it was often off by a few seconds (e.g. 00:14:57.192).

5.0 DATA REMARKS

Discussed in Sections 3.0 and 4.0.

Quicklook images of the dataset can be found at:

http://radarmet.atmos.colostate.edu/name/composites/

6.0 REFERENCES

Barber, Dobkin, and Huhdanpaa, 1996: The quickhull algorithm for convex hulls. *ACM Transactions on Mathematical Software*, **22**, 469-483.

Battan, L. J., 1973: *Radar Observation of the Atmosphere*. University of Chicago Press, 324 pp.

Bringi, V. N., and V. Chandrasekar, 2001: *Polarimetric Doppler Weather Radar: Principles and Applications*. Cambridge University Press, 636 pp.

Bringi, V. N., T. Tang, and V. Chandrasekar, 2004: Evaluation of a new polarimetrically based Z-R relation. *J. Atmos. Oceanic. Technol.*, **21**, 612-623.

Cifelli, R. W.A. Petersen, L.D. Carey, and S.A. Rutledge, 2002: Radar Observations of the Kinematic, Microphysical, and Precipitation Characteristics of Two MCSs in TRMM-LBA. *J. Geophys. Res*, **29**, 10.1029/2000JD0000264.

Doviak, R. J., and D. S. Zrnic, 1993: *Doppler radar and weather observations*. Academic Press, 562 pp.

Giangrande, S. E., and A. V. Ryzhkov, 2005: Calibration of dual-polarization radar in the presence of partial beam blockage. *J. Atmos. Oceanic. Technol.*, **22**, 1156-1166.

Patterson, V. L., M. D. Hudlow, P. J. Pytlowany, F. P. Richards, and J. D. Hoff, 1979: GATE radar rainfall processing system. NOAA Tech. Memo. EDIS 26, NOAA, Washington, DC, 34 pp. [Available from National Technical Information Service, Sills Building, 5285 Port Royal Road, Springfield, VA 22161.].

Tessendorf, S. A., L. J. Miller, K. C. Wiens, and S. A. Rutledge. 2005: The 29 June 2000 supercell observed during STEPS. Part I: Kinematics and microphysics. *J. Atmos. Sci.*, **62**, 4127–4150.